Topographical and mechanical characterization of living eukaryotic cells on opaque substrates: development of a general procedure and its application to the study of non-adherent lymphocytes

Rafael Daza , Julia Cruces , María Arroyo-Hernández , Núria Marí-Buyé , Mónica De la Fuente , Gustavo R Plaza , Manuel Elices , José Pérez-Rigueiro and Gustavo V Guinea

Keywords: atomic force microscopy, cell, mechanics

Abstract

The mechanical behavior of living murine T-lymphocytes was assessed by atomic force microscopy (AFM). A robust experimental procedure was developed to overcome some features of lymphocytes, in particular their spherical shape and non-adherent character. The procedure included the immobilization of the lymphocytes on amine-functionalized substrates, the use of hydrodynamic effects on the deflection of the AFM cantilever to monitor the approaching, and the use of the jumping mode for obtaining the images. Indentation curves were analyzed according to Hertz's model for contact mechanics. The calculated values of the elastic modulus are consistent both when considering the results obtained from a single lymphocyte and when comparing the curves recorded from cells of different specimens.

1. Introduction

The mechanical interaction between cells and their environment plays a leading role in critical aspects of their life, as shown by an ever increasing number of discoveries in modern biology (Butcher *et al* 2009, Raman *et al* 2011). Cells may alter their orientation, shape, internal constitution, contract, migrate, adhere, modify the synthesis and degradation of extracellular constituents, or even their life cycle in response to perturbations in their mechanical environment (Zhu *et al* 2000). Although there exist a large number of techniques to assess the mechanical behavior of living cells (micropipette aspiration (Mitchison and Swann 1954), optical tweezers (Henon *et al* 1999) and magnetic twisting cytometry (Wang *et al* 1993, among others), Atomic force microscopy (AFM) is the only one that combines the measurement of mechanical properties and cell imaging.

Since the beginning of this technique (Binnig *et al* 1986), AFM has proven to be a powerful tool for the structural characterization of materials and systems at the nanoscale. In the field of Biology, AFM allows acquiring high resolution images in the range of nanometers (Addae-Mensah and Wikswo 2008), far beyond other techniques such as optical or scanning electron microscopy. In addition, the possibility of working in a liquid environment allows studying life constituents under conditions close to the physiological ones (Ando *et al* 2008, Bippes and Muller 2011). Finally, AFM ability to measure forces and deformations makes it a valuable tool for characterizing protein (Steward 2002), cell (Radmacher *et al* 1996, Benoit and Selhuber-Unkel 2011) and tissue (Loparic *et al* 2010) mechanical responses.

The usual AFM configuration combines cell immobilization on a transparent substrate and the use of an inverted light microscope to initially position the AFM cantilever (Costa 2006). Although there are authors who used the tapping mode for cell imaging (Putman *et al* 1994, LeGrimellec *et al* 1997, Vie *et al* 2000), measurements are usually run in the contact mode (Benoit *et al* 1997, Braet *et al* 1998, Müller and Dufrene 2011). However, this configuration is largely inadequate for the characterization of the interaction between cells and biomaterials, since most of them are opaque and the advantage of observing simultaneously the cell and the AFM cantilever offered by the inverted light microscope setup is lost.

In addition, the use of AFM contact mode—which keeps constant the deflection of the cantilever around a few nanometers (Putman *et al* 1994) may apply large forces on the samples and lead to undesired effects in soft systems. In particular, this mode can displace cells or even inflict severe damage on them upon observation. Although this could be minimized through the use of low cantilever deflections, the unavoidable drift in the zero force level (see below) difficults its implementation.

By contrast to contact mode, the AFM jumping mode (Pablo *et al* 1998) works as a sequence of individual deflection versus distance curves at each point of the sampled surface: the tip in contact with the surface is vertically retracted prior to lateral displacement avoiding shear forces on the sample. However, the displacement and force data are not recorded for the sake of getting a faster measurement. Therefore, since these data are not available, it is not possible to make a post-processing of the data in order to extract information about mechanical properties of the sample as it could be done with other modes such as quantitative imaging (Chopinet *et al* 2013, Dhahri *et al* 2013). Like contact mode, in jumping mode the normal force is referred to a zero force level that may change during the scan. However, since the tip is moving in and out of contact, a simple algorithm can be used to continuously reset the zero force level at the largest distance from the sample, ensuring a constant value of the set point. This feature is particularly appropriate for a careful control of the forces applied to biomolecules. Moreno-Herrero *et al* (Moreno-Herrero *et al* 2004) established that jumping mode is a well-positioned mode to image small biological samples such as DNA, molecules or viruses. Additionally, as described below, AFM jumping mode allows monitoring the hydrodynamic effects experienced by the tip when displaced in a liquid environment (Butt *et al* 2005). These effects are used in this work to improve the approaching step of AFM measurements.

Lymphocytes provide an adequate case of study for the development of general AFM observation techniques and mechanical assessment of living cells due to their intrinsic interest as key players in the immune system, their low adherence to substrates and their easy availability. Lymphocytes determine the specificity of the immune response to infectious microorganisms and other foreign substances and are divided into two groups, B and T, depending on the organ in which maturation occurs. All lymphocyte precursors are produced in the bone marrow but T-lymphocytes, which are the subject of this work, mature in the thymus (Abbas *et al* 1994) and are subsequently released in the circulatory system, where they remain circulating until the recognition of their specific antigen. Therefore, unlike typical adherent cells such as fibroblasts or macrophages, T-lymphocytes do not interact readily with most surfaces (Gupta *et al* 1999). Although this feature simplifies the isolation of T-lymphocytes from other immune cells (Russo *et al* 1979) it hampers AFM observation, where cell immobilization is a pre-requisite. Consequently, the vast majority of studies on lymphocytes resort to cell fixation procedures, despite the possible alterations introduced by these methods.

Several works on fixed cells have found significant differences in the adhesion forces of fixed and non-fixed lymphocytes (Wu *et al* 2009) and reported dependence of cell morphology upon adhesion (Cai *et al* 2010). These facts highlight the need to develop new procedures that allow the immobilization and observation of living lymphocytes without altering their morphology and mechanical properties. These procedures could, in principle, be easily transferred to other non-adherent cell lineages (Kato *et al* 2003) such as human T cell lymphoma Jurkat, human B cell leukemia Daudi or mouse myeloid 32D cells.

In this paper, a novel procedure that allows simultaneous imaging and measurement of the mechanical properties of non-adherent living cells on opaque substrates is presented. This new method includes the use of functionalized substrates for immobilizing cells, exploits hydrodynamic forces for monitoring the approach to cells, and uses the jumping mode for performing the measurements. To evaluate the performance of the new procedure, we have applied it to the observation of T-lymphocytes, cells that suffer clearly visible morphological changes when brought to contact with activating surfaces (Rodriguez and Anderson 2010).

2. Materials and methods

2.1. Substrate preparation

Monocrystalline silicon (p-doped, $\rho = 0.1$–$0.5\,\Omega$ cm) substrates were biofunctionalized by activated vapor silanization (AVS) (Arroyo-Hernandez *et al* 2008), which combines vapor silanization and chemical vapor deposition, and results on a large density of amine groups on the surface (Lyubchenko *et al* 1992). Prior to biofunctionalization, substrates were cleaned by sequential sonication in acetone and ethanol for five minutes, dried with an argon flow and introduced into the AVS reactor. The AVS technique is explained elsewhere (Arroyo-Hernandez *et al* 2003, 2006, 2008, 2014, Martin-Palma *et al* 2004). Briefly, 3-aminopropyltriethoxysilane (APTS) (Sigma-Aldrich) was vaporized at 150 °C at low pressure ($<5 \times 10^{-2}$ mbar) and activated to 750 °C before entering the treatment chamber in which the substrate was located. The substrate was exposed to APTS vapor for 20 min. Process parameters such as evaporation and activation temperatures, working pressure or deposition time were chosen to result in homogeneous films, with a high concentration of amines at the surface of the substrate (Arroyo-Hernandez *et al* 2014).

2.2. Cell obtaining and preparation

We have used female ICR-CD1 mice (*Mus musculus*), which were obtained from Janvier S.A.S. (Le Genest-St-Isle, France) at the age of 7–8 months. They were specific pathogen-free, according to the Federation of European Laboratory Science Associations recommendations. Mice were randomly housed in groups of five individuals per cage (50×25 cm polyurethane boxes), at a constant temperature (22 ± 2 °C) in sterile conditions inside an aseptic air negative-pressure environmental cabinet (Flufrance, Cachan, France), on a 12/12 h reversed light/dark cycle (lights on at 8:00 h, off at 20:00 h). Mice had access to tap water and standard Sander Mus pellets (A04 diet from Panlab L. S. Barcelona, Spain) *ad libitum*. This diet was in accordance with the recommendations of the American Institute of Nutrition for laboratory animals. Mice were marked for their individual follow-up. The experimental protocol was approved by the Animal Ethics Committee of the Universidad Complutense de Madrid (Spain). Animals were treated according to the guidelines of the European Community Council Directives 1201/2005 EEC.

Peritoneal leukocytes were obtained from mice at the age of 12 ± 1 months, between 8:00 and 10:00 h, without sacrificing the animals. Each mouse was held by its cervical skin, the abdomen was cleansed with 70% ethanol and, subsequently, 3 ml of sterile Hank's solution (Sigma-Aldrich, Tres Cantos, Spain), previously tempered at 37 °C, was injected intraperitoneally. After massaging the abdomen, 80% of the injected volume was recovered. Peritoneal leukocytes were counted in Neubauer chambers (Blau Brand, Germany). Cellular viability was routinely checked by the Trypan Blue (Sigma, St Louis, MO) exclusion test, and only suspensions with cell viability higher than 99 ± 1% were used. Cells were maintained at 4 °C throughout the performance of experimental protocols.

In order to isolate the non-adherent lymphocytes from the peritoneal leukocyte population, the suspension obtained from each mouse was incubated at 37 °C in a humidified atmosphere of 5% CO_2, for 45 min using migratory inhibitory factor plates (Kartell, Noviglio, Italy). After this time the supernatants, mainly constituted by non-adherent lymphocytes, were collected using a Pasteur pipette. Lymphocytes were identified by their morphology and quantified in Neubauer chambers using optical microscopy (x40). Additionally, the purity of lymphocyte suspension was confirmed by immunostaining with monoclonal antibodies for the expression of CD45, CD3 and CD19 (BD Pharmingen, San Diego, CA), conjugated with different fluorochromes. The fluorescence was measured using a flow cytometer (FACSCalibur; Becton Dickinson, Franklin Lakes, NJ). The results were analyzed with Cell Quest Pro software (BD Biosciences, San Jose, CA). The percentage of T lymphocytes obtained after the isolation protocol used for the subsequent experiments was higher than 86%.

Starting lymphocyte concentration was set at 2.5×10^5 cell ml^{-1}. All samples were subjected to vortex stirring in order to ensure a homogeneous cell distribution. Samples were labeled from S1 to S8, each corresponding to an individual. A volume of 100 μl was deposited on the functionalized silicon surface used as substrates for AFM observation and cells were incubated on the substrate for two hours at nominal conditions 25 °C and 40% relative humidity. Finally, cells not attached to the surface were removed by rinsing with filtered Hank's solution.

2.3. SEM measurements

Lymphocytes were fixed with 4% (w/v) gluteraldehyde (Sigma-Aldrich) in phosphate buffer solution (PBS) for 1 h at room temperature. After fixation, the substrates were gently washed with PBS and progressively dehydrated. For this purpose, samples were consecutively immersed for 10 min in ethanol solutions of 30, 50, 70, 80, 90, 96 and 100% (v/v) (in the last one, samples were immersed twice). Once dehydrated, the cell cultures were dried using a CO_2 critical point dryer (Polaron, CPD7591, East Sussex, UK), where ethanol was slowly exchanged with CO_2 and the sample dried at the critical pressure and temperature of CO_2. Finally, the samples were sputter-coated with gold using the equipment Emitech K550X, sputter coarter (90 s, 20 mA) (East Sussex, UK) and examined with a FESEM Auriga Zeiss (Cambridge, UK) scanning electron microscope at 4 kV.

2.4. AFM measurements

A Cervantes AFM (Nanotec Electrónica S. L., Madrid, Spain) was utilized for imaging and mechanical characterization of lymphocytes. We used relatively soft cantilevers (Olympus OMCL-RC800) with spring constants of about $k_c = 0.05$ Nm^{-1} as determined by the Sader method (Sader *et al* 1999), half-cone angle of $\theta = 39°$ (measured in our laboratory from SEM images, FESEM Auriga Zeiss) and tip radius of 15 nm (measured in our laboratory from SEM images, FESEM Auriga Zeiss). Each cantilever was cleaned in ethanol before use. AFM cell imaging experiments were performed in liquid environment in the jumping mode (Pablo *et al* 1998) with a value of the normal force set point that is equivalent to 0.2 nN.

The utilization of an opaque substrate impeded simultaneous observation by light microscopy of the AFM tip and the cell. Consequently, a novel approach based on the hydrodynamic forces developed during the cantilever displacement was devised. This procedure requires continuous monitoring the force on the cantilever as it approaches the sample, as sketched in figure 1(a). Therefore, the normal force and the voltage exerted on the piezo-actuator were monitored simultaneously and recorded by means of an

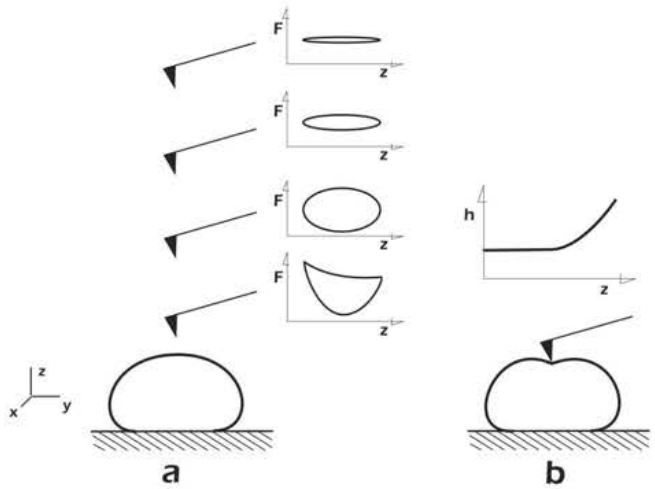

Figure 1. The tip-approaching procedure and deflection–displacement curve. (a) The tip-approaching procedure is based on the shape of the F–z hysteresis loop due to the hydrodynamic forces suffered by the tip–cantilever system. When the tip approaches the sample, the loop enlarges, finally modifying its elliptical shape when contact is imminent. (b) Sketch of deflection–displacement curve recorded on a soft sample.

oscilloscope. Representation of these data as a function of the time while piezo-actuator executed the characteristic cyclic movement of the jumping mode; led to the acquisition of loops as sketched in figure 1(a). Far from the sample, the force shows a small hysteresis loop, which monotonically enlarges as the sample is approached. When contact is finally established between tip and cell the effect is clearly observable from a considerable change of the shape of the hysteresis loop, since an increase in the normal force is observed. Additionally, the retracting part of the loop also changes due to the presence of a small adhesion region. The relation between the shape and size of the hysteresis loop and the tip–sample distance permits an accurate approaching.

Once the tip–substrate distance was optimized to allow cell detection without cell displacement, the scanning stage was started. When a lymphocyte was found, the scanning area was centered on it and a high-resolution image (256×256 pixels) was taken. A closed-loop system was used in order to prevent the effects of the drift during scanning. Initial selection of the scanning areas with lymphocytes was done with the use of a reflection light microscope.

After recording the whole image, the scanning was stopped and the mechanical response was assessed by means of cantilever deflection versus piezo-actuator displacement curves taken at selected points (a sketch of the aspect of these curves is shown in figure 1(b)). These curves record cantilever deflection (h), as a function of the piezo-actuator displacement normal to the substrate (z displacement). More than 30 curves were obtained on each cell. Each h–z curve consisted of 512 sampling points and was obtained at a constant loading rate of 1 μm s^{-1}.

Once the curves for each cell were obtained, five additional indentation tests were performed on the silane-coated silicon substrate. The elastic modulus of the coating was determined from nanoindentation tests as 20 GPa, much larger than the elastic modulus of the cells. Since the substrate is significantly stiffer than the cantilever, it is assumed that the tip does not indent it and, consequently, the z displacement coincides with the deflection of the cantilever, h. The slope of the linear post-contact region provides the conversion factor (optical sensitivity or detector sensitivity) to convert the cantilever photodetector signal into deflections. To prevent the samples from drying during the measurements, two small recipients were filled with water and placed near the AFM head, and all the set-up was covered with a bell cover.

Before and after recording h–z curves, cell images were acquired to discard those curves in which cells were displaced as a consequence of the measuring process. The surface structure of lymphocytes was analyzed by means of topography and normal force images in the jumping mode. The processing of the AFM images consisted of simple equalizing and adjusting the contrast and the brightness of the micrographs with the WSxM program (Nanotec Electrónica, Spain) (Horcas *et al* 2007).

2.5. Indentation of lymphocytes

Figure 2 shows a simplistic sketch of the main displacements involved in the indentation process: the piezo-actuator displacement z, the cantilever-deflection h, and the indentation depth δ.

The initial state is displayed in figure 2(a) (z_o, h_o, $\delta = 0$). After moving the piezo-actuator with a *rigid* sample, the situation is sketched in figure 2(b) (z, h_1, $\delta = 0$), where $z - z_o = h_1 - h_o$. If the sample is soft and can be indented, the cantilever deflection will be less than the previous situation, and the indentation depth δ will be given by

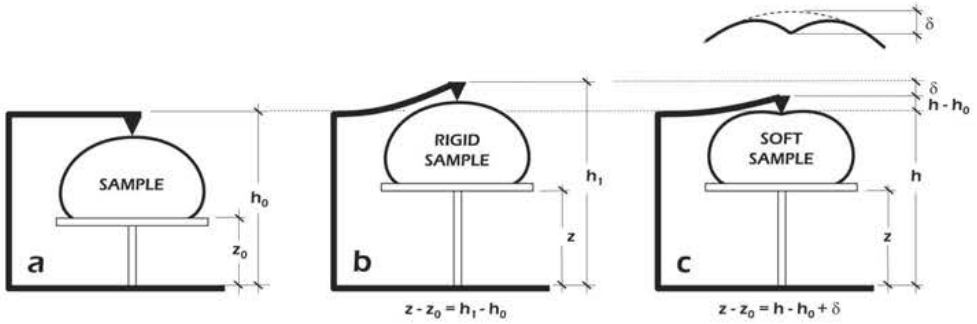

Figure 2. Sketch of the main displacements involved in the indentation process. The piezo-actuator displacement z, the cantilever-deflection h, and the indentation depth δ. (a) z_o and h_o are piezo-actuator position and cantilever deflection when sample is brought into contact with the tip. (b) If the sample is stiffer than the cantilever, z piezo-actuator displacement coincides with the deflection of the cantilever. (c) Otherwise, the sample can be indented and the indentation depth is given by $\delta = (z - z_o) - (h - h_o)$.

$$\delta = (z - z_o) - \left(h - h_o\right) \tag{1}$$

as shown in figure 2(c).

The relation between the indentation force F and the indentation depth δ can be obtained taking into account that:

- If the cantilever behaves elastically, the force on the tip is given by:

$$F = k_c\left(h - h_0\right), \tag{2}$$

where k_c is the cantilever stiffness. Equations (1) and (2) are used to transform h–z in $F - \delta$.

- If the sample behaves elastically, with an initial elastic modulus E, the force exerted by the indenter may be written—as a zeroth order approximation and assuming that tip geometry is a perfect pyramid without blunted apex-by the Hertz's elastic model for contact (Hertz 1882, 1896, Dimitriadis *et al* 2002, Rico *et al* 2005), i.e.:

$$F = k_S\ \delta^2, \tag{3}$$

where k_S is given by $k_S = E^{'} \tan\theta/2^{1/2}$, θ is the cantilever tip semiangle and $E^{'}$ the plane strain elastic modulus $(E/\left(1 - \nu^2\right))$, where ν, the Poisson coefficient, is assumed to be 0.5 as cells are considered incompressible.

Hence, equating expressions equations (2) and (3) a relation between the piezo-actuator displacement z and the elastic modulus of the sample, E, can be obtained, i.e.:

$$k_c \cdot \left(h - h_0\right) = k_S\,(E)\,\delta^2(z, h). \tag{4}$$

Knowledge of z (by controlling the piezo-actuator displacement) and of h (by measuring the cantilever deflection) allows computing the elastic modulus E.

In the pre-contact region, where the cantilever tip and the cell are not in contact, the cantilever deflection h is constant, equal to h_0. Therefore, the general $h - z$ relationship can be written as:

$$h = \begin{cases} h_o & z < z_o \\ h_o + \dfrac{k_S(E)}{k_c}\left[(z - z_o) - \left(h - h_o\right)\right]^2 & z \geqslant z_o \end{cases} \tag{5}$$

3. Experimental results

3.1. Morphology of lymphocytes

Figure 3(a) shows a representative AFM image of a lymphocyte. Structural details that could be assigned to pseudopodia can be observed whereas lamellipodia are not present. Pseudopodia are also clearly visible in figure 3(b), where a scanning electron microscopy of a fixed lymphocyte is shown for comparison. Wu *et al* (Wu *et al* 2009) related the presence of lamellipodia to activated lymphocytes and, consequently, our results suggest that lymphocytes were not activated either during sample preparation or AFM observation, a process that takes 4–5 h. AFM images of a lymphocyte recorded before the acquisition of a great number of deflection–displacement curves and after it can be observed in figures 3(c) and (d).

These results suggest that cell–surface interaction is stable and does not induce any observable change in the lymphocytes. It is worth stressing that the images and data presented in this work were acquired on living cells immersed in Hank's solution without employing a fixative protocol. To the best of the authors' knowledge, this is the first time that these data were obtained using living functional lymphocytes.

3.2. Nanomechanical properties of the lymphocytes

The mechanical behavior of the lymphocytes was characterized from the deflection–displacement curves obtained as described above. Representative experimental deflection–displacement data in form of force–indentation depth are shown in figure 4(a), which compares five force–indentation curves out of thirty taken on the same lymphocyte. As the curves exhibit almost the same shape, we can assume that

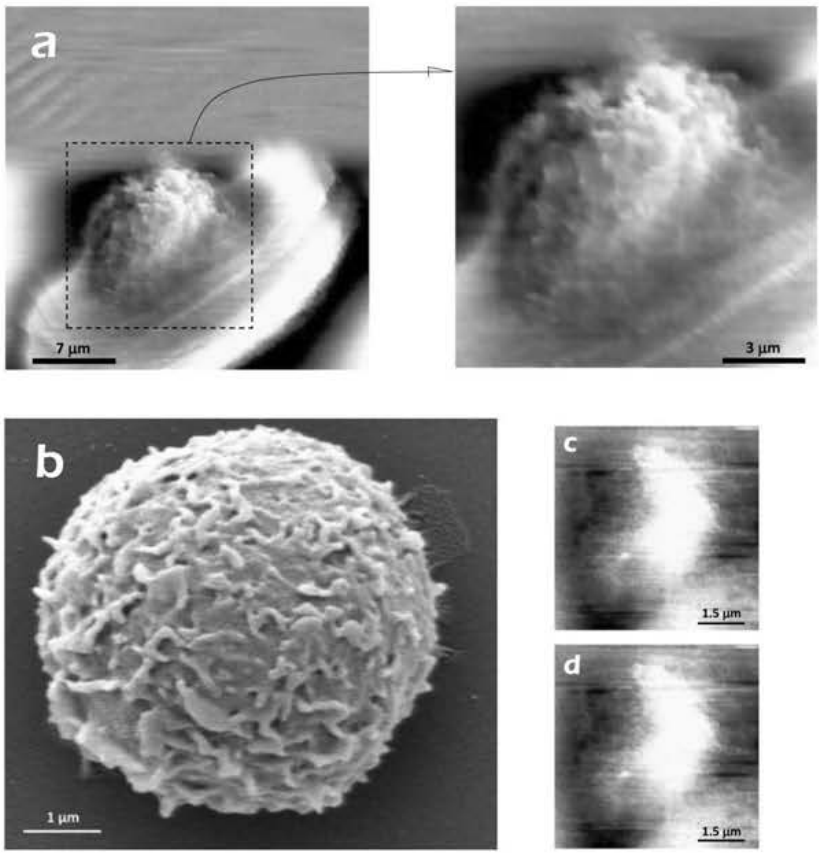

Figure 3. Image of a T-lymphocyte. (a) AFM normal force image (the halo around the cell is attributed to a mechanical contact between cell and cantilever) and enlarged-view of the selected area. (b) SEM image of a fixed T lymphocyte. Pseudopodia are detectable in all images. (c) and (d) AFM images of a T-lymphocyte that were recorded before the acquisition of more than 150 deflection–displacement curves and after it, respectively.

repeated indentation did not cause sensible damage on the lymphocyte. It is interesting to note that the forces exerted by the tip did not exceed 1.5 nN.

The reproducibility of the method can be also deduced from figure 4(b) where representative force–indentation depth curves from different individuals are shown. All of them show a similar shape with different stiffness, as reflected in table 1. Table 1 lists the values obtained for the elastic modulus from Hertz's equation in the form of mean ± standard error, and their statistical distribution is shown in figure 5 with box plots.

Table 1 lists the values obtained for the elastic modulus from Hertz's equation in the form of mean ± standard error.

3.3. Determination of the point of contact and the origin of the deflection–displacement curve

The characterization of the mechanical properties of cells by AFM presents some problems and limitations. Specifically, the determination of the contact point between tip and cell during the indentation test is a key issue for the determination of the elastic modulus and the right representation of all the force–indentation curve. Although some works proceeded by visually selecting the contact point, a few more objective procedures were proposed (Costa 2006, Crick and Yin 2007, Benitez *et al* 2013).

Figure 6 shows a typical deflection–displacement (h–z) curve of a lymphocyte subjected to an indentation test. The curve exhibits two different regions: (1) pre-contact region ($z < z_o$), where tip and cell are not in contact and, consequently, the cantilever deflection is constant and (2) a post-contact region ($z > z_o$) where deflection depends on the cantilever-cell stiffness ratio. The boundary between those regions is the contact point (z_o, h_o) shown in the figure 6. Identification of this point represents a major difficulty in the analysis of the curve, since for soft samples such as cells, it is not characterized by a noticeable increase in stiffness.

In this work, we have used a nonlinear least-squares fit to equation (5) based on the Levenberg–Marquardt algorithm (Moré 1978). This method has allowed us an accurate determination of the elastic modulus E, and the tip-cell contact point z_o and h_o.

4. Discussion of experimental results and final comments

In this work we present a procedure that solves part of the problems related with the use of AFM for

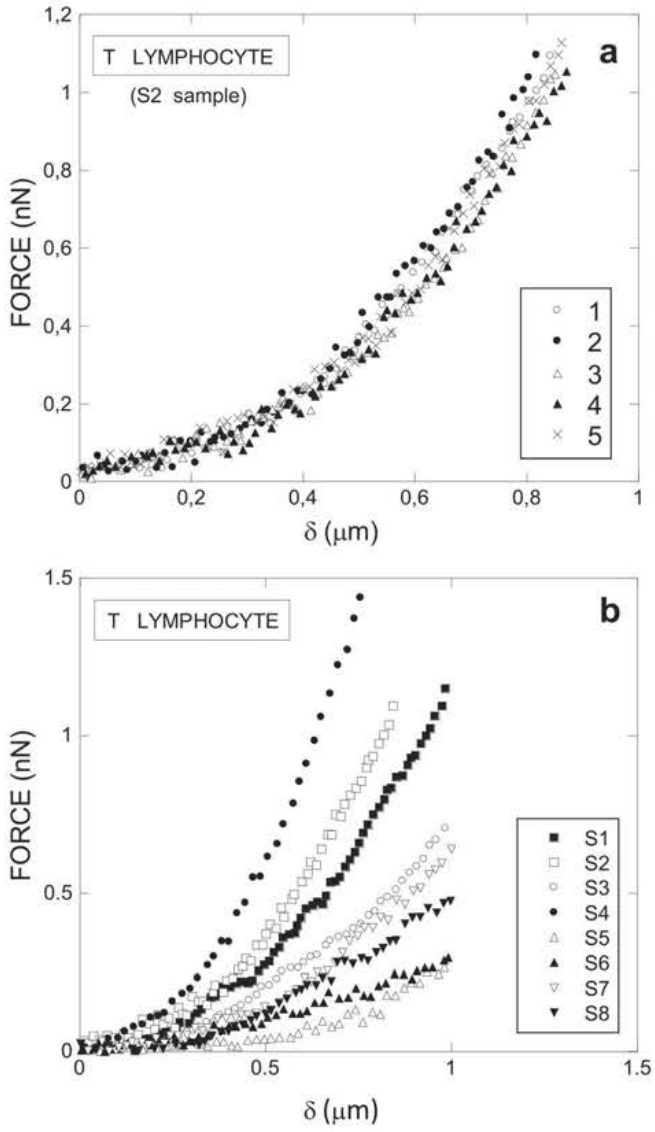

Figure 4. Force–indentation depth curves. (a) Curves measured on the same T lymphocyte from the S2 individual. (b) Force–indentation depth curves for different individuals.

Table 1. Estimated Elastic Modulus.

Specimen	Elastic Modulus (kPa)
S1	1.9 ± 0.1
S2	2.26 ± 0.08
S3	1.12 ± 0.03
S4	3.3 ± 0.8
S5	0.23 ± 0.06
S6	0.48 ± 0.03
S7	0.87 ± 0.03
S8	0.54 ± 0.09

characterizing the mechanical properties of cells. Since its introduction in the field of Biology, AFM has demonstrated its aptitude to acquire images with high resolution on the order of nanometers. Besides, the possibility of working under different environments, —including those that support living cells—allows to address the study of the principal life constituents in conditions similar to those found *in vivo*. According to these capabilities, AFM was applied to obtain images and to study the mechanical response of a wide variety of biological structures ranging from proteins and cell organelles to cells and tissues.

Although the combination of AFM and inverted optical microscopy has represented an unquestionable improvement in the area of cell mechanics, that provides a great control of the experimental process and enlarges the technical capabilities, the characterization of large cells on opaque substrates, as it occurs in cells on implanted biomaterials, represents a major challenge for AFM.

4.1. Cell Immobilization

The simultaneous imaging and mechanical testing of the cells requires the sample remaining immobile during the imaging scan and the measurement of force–indentation curves and, additionally, that cells are not activated as a consequence of the interaction of

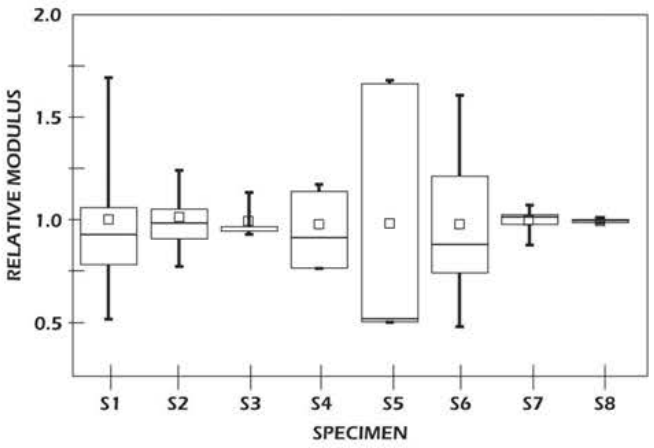

Figure 5. Box plot representation of the relative elastic modulus $E_i/\hat{E}$. The relative modulus is computed as the ratio between the elastic modulus obtained in a measurement and the average for the corresponding lymphocyte. The bottom and top of the box indicate the first and third quartiles, and the band inside the box the second quartile (the median). The lines extending vertically from the boxes represent the minimum and the maximum of all of the data. A square inside of the box represents the mean of the data. The label of each specimen is shown on the *x*-axis. Individuals are identified as in figure 4(b).

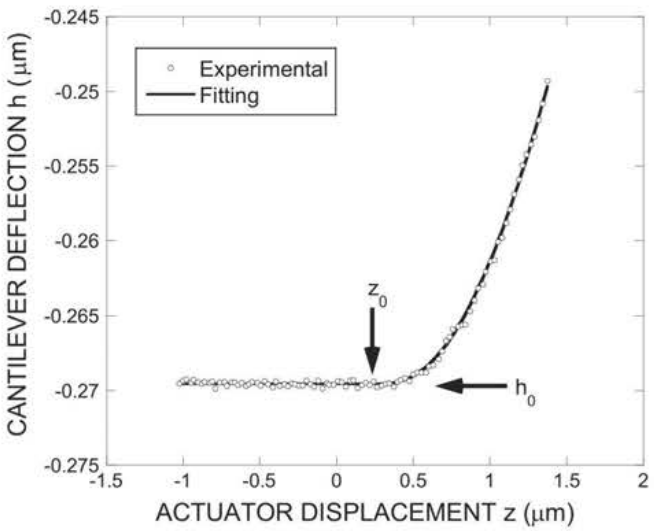

Figure 6. Representative deflection–displacement curve. Representative deflection–displacement curve recorded on a T lymphocyte. The contact point coordinates (shown in the figure) were determined by fitting the experimental data to the Hertz's model equation.

the cell with the substrate (Hu *et al* 2009). Probably, the difficulty in finding a substrate with appropriate surface interaction is one the reasons why there are few published studies on lymphocyte observation by AFM. In fact, in previous works, their mechanical properties were analyzed using fixed cells with a similar protocol to that used for preparing SEM samples (Wu *et al* 2009), assuming that these fixing protocols kept the structural aspects of the cells, and that the measured mechanical properties were representative of those of the living cells. However, different researchers found that this kind of protocol could increase the cell elastic modulus value (Braet *et al* 1998) and cause distortion in surface detail (Boyde *et al* 1972).

Therefore, in order to extend AFM techniques to non-adherent cells, our new methodology includes the functionalization of substrates, so that cells can be characterized without resort to fixing protocols. Lymphocytes can be observed immersed in a buffer or in a cell culture medium ensuring the cell survival in the course of the experiments and the non-disturbance of their response.

Functionalized silicon surfaces obtained by the AVS technique were previously characterized as biocompatible surfaces (Arroyo-Hernandez *et al* 2006) keeping the biological functionality of biomolecules. This was the reason to use them as substrates for the immobilization of lymphocytes. As shown above, lymphocytes immobilized in these substrates can be imaged with an exceptional resolution (figure 3), being possible to resolve structures compatible with pseudopodia, a representative structure of T-lymphocytes membrane. This fact, in combination with the

total absence of lamellipodia, suggests that the cell–substrate binding was stable, and lymphocytes were neither displaced during the scan nor during indentation tests. No direct evidence of the interaction responsible for lymphocyte immobilization on the functionalized substrates was found. Presumably, the electrostatic attraction between the positively charged amine groups and the negatively charged cell membrane (Marikovsky *et al* 1978) is the main reason for this effect.

4.2. Strategy for approaching the tip

One of the key steps of this novel procedure was the development of a new technique to approach the tip to the sample. This method exploits the variation of the hydrodynamic forces exerted on the cantilever tip when approaching a submerged obstacle. It has been shown that the force exerted on the cantilever increases not only proportional to velocity, but also inversely proportional to the mass of liquid between tip and obstacle (Butt *et al* 2005). It is found that this force has a repulsive character during approaching and an attractive character during retreating.

As a consequence of this hydrodynamic force, the approaching and retracting parts of deflection curves are not identical when the cantilever is immersed in liquid showing a hysteretic behavior. Since the jumping mode allows acquiring force–distance curves at each point of the image, the hysteresis cycle will appear naturally in this observation mode. Besides, the size of the hysteresis cycle grows as the distance between tip and sample tends to zero. Figure 1(a) sketched this phenomenon. Ortega-Esteban *et al* (Ortega-Esteban *et al* 2012) developed a method which allows eliminating the presence of these cycles in a numerical way making the image acquisition process more controllable. Although this method supposes an evident improvement in the jumping mode, however, we decided to not use it in order to keep the original cycle shape. Based on initial calibrations, it is possible to acquire a broad knowledge of the general aspect of the hysteresis cycles as a function of the tip-substrate distances that, in turn, allows stopping the approach movement at a given tip–sample distance. With this procedure, the lateral displacement of the cells as a consequence of AFM scanning is prevented.

4.3. Advantages of using the jumping mode

The results presented above illustrate the advantages of using the jumping mode over the usual contact mode for the characterization of cells. Typically, cell images are acquired by means of the contact mode, despite it is demonstrated that huge shear forces are applied on the cell surface, even with soft cantilevers (Putman *et al* 1994, Tang and Ngan 2011, Zhou *et al* 2012). Shear forces could break the cell–substrate binding or even damage the cell surface. In contrast, the jumping mode reduces the tip–sample contact time and, since the tip is moved laterally when both are far apart, shear forces are minimized. Moreno-Herrero *et al* (Moreno-Herrero *et al* 2004) made a comparative study between contact, tapping and jumping modes for imaging biological samples in liquids, and established that jumping mode is adequate for imaging small biological samples such as DNA molecules (Moreno-Herrero *et al* 2003) or viruses. The present work extends that the advantage of using the jumping mode to the analysis of cells.

Another advantage of the jumping mode is the possibility to correct the drift that affects the zero position of the cantilever deflection at long observation times. The main effect of the drift is the change in the applied force on the cell, which may increase during the measurements. In order to avoid this effect, the jumping mode allows a correction that establishes a set point relative to zero deflection in every cycle, preventing large variations of the force. As indicated above, the jumping mode also offers a convenient way to perform the approaching step, which is key to extend the AFM technique to such large cells as lymphocytes.

4.4. Indentation depth and cell stiffness

Another problem in the quantification of the cell mechanical behavior lies in the use of sharp cantilever tips that may induce local strains exceeding the linear initial material regime. Dimitriadis *et al* (Dimitriadis *et al* 2002) suggested that this effect is relevant when non-spherical tips are used. As the geometry of the tip used in this work was pyramidal, we expanded our study to assess this effect. The value of elastic modulus was estimated with Hertz's model considering different values of indentation depth (figure 7). As it can be seen in this figure, the value of the elastic modulus decreases as indentation depth increases until a depth of 500 nm is reached. From this point on the elastic modulus remains constant up to a value of 1200 nm. Deeper indentations yield an increase in the elastic modulus, probably reflecting the effect of the underlying substrate. Consequently, it is possible to establish a range of indentation depths from 500 to 1000 nm in which the elastic modulus remains constant. Indentation depths deeper than 1000 nm were not taken into account for the determination of the elastic modulus.

The large values of the elastic modulus at small indentation depths observed in figure 7 are usually owing to two different causes: the repulsive interaction between the tip and different cell membrane constituents (Rico *et al* 2005) and the errors in the determination of the contact point. Similar trends were found in the analysis of polymer gels (Dimitriadis *et al* 2002), cells (Rico *et al* 2005) or even actin fibers (Lan *et al* 2008). Whereas it is not possible to reduce the effect of the repulsive interaction, all these studies show that the contribution due to inappropriate choice of contact point decreases as one uses larger indentation depths. This effect can be observed in

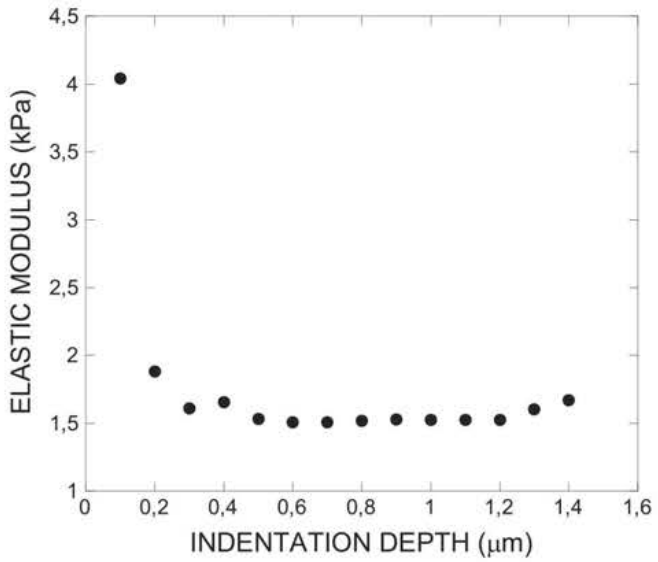

Figure 7. Evolution of the estimated elastic modulus with the indentation depth selected for the fitting. The value of the elastic modulus decreases as indentation depth increases until a depth of 500 nm is reached. From this point on the elastic modulus remains constant up to a value of 1200 nm. Deeper indentations yield an increase in the elastic modulus, probably reflecting the effect of the underlying substrate. Consequently, it is possible to establish a range of indentation depths from 500 to 1000 nm in which the elastic modulus remains constant.

figure 7 where the elastic modulus is clearly overestimated at small indentation depths whereas it approaches a steady value as indentation is increased.

Crick *et al* (Crick and Yin 2007) established that if the contact point is missed by less than 50 nm, the calculated material properties for small indentations are erroneous, although it can be partially solved by indentations beyond 200 nm, that asymptotically tend to the correct estimate of material stiffness. Also, their numerical simulations for linear materials established that when the contact point in missed in 50 nm, the calculated elastic modulus reaches its actual value for indentation depths around 500 nm. Taking as a reference these results, we can assume that our routine missed the contact point by less than this quantity and knowing that does not exist lost of linear response, we used an interval of data of depths ranging from zero to one micron in order to estimate the elastic modulus of lymphocytes in the most precise way. Although *a priori* these indentation depths could seem extremely large, since the height of the tip is 2.9 μm and the deflection–displacement curves were taken in the highest part of the cells, this geometry does not allow a direct contact between the cantilever and the cell. Consequently, the cell contacted exclusively with the tip, preventing an overestimation of the value of the elastic modulus related to additional spurious contact (Harris and Charras 2011). In this context, the use of a spherical tip would allow a more straight forward analysis, since Hertz model can be applied for this type of indenters up to large values of strain (Yofee 1984). In our case, the requirement of obtaining an image of the cell prior to indentation implied the use of pyramidal tips. The overall strain of the cells is below the admitted value of 20% (Dimitriadis *et al* 2002) (1 μm deformation in approximately 7 μm of initial length of the cell), so that Hertz model can in principle be applied. Pyramidal geometry, however, might imply larger strains of the cell close to the tip that might render the values of E obtained from Hertz model somewhat inaccurate. In any case, application of this procedure allows, at the very least, an easy and precise comparison of the elastic modulus of the different cells that were analyzed.

In addition, the similarity of all the curves showed in figure 4 suggests that lymphocytes were not affected by indentation. The high reproducibility of the results emphasizes the robustness of this new experimental procedure, including the routine used for the data fitting. Other indication of this reproducibility can be noticed in figure 5, where both the mean and median of the elastic modulus distribution appear close to one another showing that the majority of the calculated quotients tend to be concentrated around the mean value.

An accurate determination of the point of contact, the choice of the indentation depth and the use of Hertz's model for the calculation of the elastic modulus leads to results in consonance with other similar previously published (Cai *et al* 2010), and reflecting a homogeneous mechanical behavior, both at individual and intercellular level as can be seen in figures 4(a) and (b).

Acknowledgments

Dr A Gil and L Colchero (Nanotec Electrónica, S.L., Spain) offered support for AFM observations and E Baldonedo (Centro de Microscopía, UCM, Spain) for

SEM observations. The authors are grateful to Dr Y Ruiz (Real Jardín Botánico, CSIC, Spain) for her help with the drying of the cells and to José Miguel Martínez for his help with the artwork. The work was funded by MINECO Ministerio de Educación y Ciencia (Spain) through project MAT 2009-10258, BFU2011-30336, by the Comunidad de Madrid (Spain) (Grant S2011/BMD-2460) and by Fundación Marcelino Botín.

References

Abbas A K, Lichtman A H H and Pillai S 1994 *Cellular and Molecular Immunology, Updated Edition* (Amsterdam: Elsevier)

Addae-Mensah K A and Wikswo J P 2008 Measurement techniques for cellular biomechanics *in vitro Exp. Biol. Med.* 233 792–809

Ando T, Uchihashi T and Fukuma T 2008 High-speed atomic force microscopy for nano-visualization of dynamic biomolecular processes *Prog. Surf. Sci.* 83 337–437

Arroyo-Hernandez M, Daza R, Perez-Rigueiro J, Elices M, Nieto-Marquez J and Guinea G V 2014 Optimization of functionalization conditions for protein analysis by AFM *Appl. Surf. Sci.* 317 462–8

Arroyo-Hernandez M, Martin-Palma R J, Perez-Rigueiro J, Garcia-Ruiz J P, Garcia-Fierro J L and Martinez-Duart J M 2003 Biofunctionalization of surfaces of nanostructured porous silicon *Mater. Sci. Eng.* C 23 697–701

Arroyo-Hernandez M, Perez-Rigueiro J and Martinez-Duart J M 2006 Formation of amine functionalized films by chemical vapour deposition *Mater. Sci. Eng.* C 26 938–41

Arroyo-Hernandez M, Perez-Rigueiro J, Conde A, Climent A, Gago R, Manso M and Martinez-Duart J M 2008 Characterization of biofunctional thin films deposited by activated vapor silanization *J. Mater. Res.* 23 1931–9

Benitez R, Moreno-Flores S, Bolos V J and Luis Toca-Herrera J 2013 A new automatic contact point detection algorithm for AFM force curves *Microsc. Res. Tech.* 76 870–6

Benoit M, Holstein T and Gaub H 1997 Lateral forces in AFM imaging and immobilization of cells and organelles *Eur. Biophys. J. Biophys. Lett.* 26 283–90

Benoit M and Selhuber-Unkel C 2011 Measuring cell adhesion forces: theory and principles *Atomic Force Microscopy in Biomedical Research: Methods and Protocols* vol 736 (New York: Humana Press) pp 355–77

Binnig G, Quate C and Gerber C 1986 Atomic force microscope *Phys. Rev. Lett.* 56 930–3

Bippes C A and Muller D J 2011 High-resolution atomic force microscopy and spectroscopy of native membrane proteins *Rep. Prog. Phys.* 74 086601

Boyde A, Weiss R and Vesely P 1972 Scanning electron-microscopy of cells in culture *Exp. Cell Res.* 71 313

Braet F, Rotsch C, Wisse E and Radmacher M 1998 Comparison of fixed and living liver endothelial cells by atomic force microscopy *Appl. Phys.* A 66 S575–8

Butcher D T, Alliston T and Weaver V M 2009 A tense situation: forcing tumour progression *Nat. Rev. Cancer* 9 108–22

Butt H J, Cappella B and Kappl M 2005 Force measurements with the atomic force microscope: technique, interpretation and applications *Surf. Sci.Rep.* 59 1–152

Cai X, Xing X, Cai J, Chen Q, Wu S and Huang F 2010 Connection between biomechanics and cytoskeleton structure of lymphocyte and Jurkat cells: an AFM study *Micron* 41 257–62

Chopinet L, Formosa C, Rols M P, Duval R E and Dague E 2013 Imaging living cells surface and quantifying its properties at high resolution using AFM in QI (TM) mode *Micron* 48 26–33

Costa K D 2006 Imaging and probing cell mechanical properties with the atomic force microscope *Methods Mol. Biol.* 319 331–61

Crick S L and Yin F C 2007 Assessing micromechanical properties of cells with atomic force microscopy: importance of the contact point *Biomech. Model. Mechanobiology* 6 199–210

Dhahri S, Ramonda M and Marliere C 2013 *In situ* determination of the mechanical properties of gliding or non-motile bacteria by atomic force microscopy under physiological conditions without immobilization *Plos One* 8 e61663

Dimitriadis E K, Horkay F, Maresca J, Kachar B and Chadwick R S 2002 Determination of elastic moduli of thin layers of soft material using the atomic force microscope *Biophys. J.* 82 2798–810

Gupta S, Aggarwal S and Starr A 1999 Increased production of interleukin-6 by adherent and non-adherent mononuclear cells during 'natural fatigue' but not following 'experimental fatigue' in patients with chronic fatigue syndrome *Int. J. Mol. Med.* 3 209–13

Harris A R and Charras G T 2011 Experimental validation of atomic force microscopy-based cell elasticity measurements *Nanotechnology* 22 345102

Henon S, Lenormand G, Richert A and Gallet F 1999 A new determination of the shear modulus of the human erythrocyte membrane using optical tweezers *Biophys. J.* 76 1145–51

Hertz H 1882 Über die berübrung fester elasticherkörper *J. Reine Angew. Math* **92** 156

Hertz H 1896 On the contact of elastic solids ed P Lenard *Miscellaneous Papers* p 146

Horcas I, Fernandez R, Gomez-Rodriguez J M, Colchero J, Gomez-Herrero J and Baro A M 2007 WSXM: a software for scanning probe microscopy and a tool for nanotechnology *Rev. Sci. Instrum.* **78** 013705

Hu M, Wang J, Zhao H, Dong S and Cai J 2009 Nanostructure and nanomechanics analysis of lymphocyte using AFM: from resting, activated to apoptosis *J. Biomech.* 42 1513–9

Kato K, Umezawa K, Funeriu D P, Miyake M, Miyake J and Nagamune T 2003 Immobilized culture of nonadherent cells on an oleyl poly(ethylene glycol) ether-modified surface *BioTechniques* **35** 1014–21

Lan L U, Oswald S J, Ngu H and Yin F C 2008 Mechanical properties of actin stress fibers in living cells *Biophys. J.* 95 6060–71

Legrimellec C, Lesniewska E, Giocondi M C, Finot E and Goudonnet J P 1997 Simultaneous imaging of the surface and the submembraneous cytoskeleton in living cells by tapping mode atomic force microscopy *C. R. Acad. Sci.* II 320 637–43

Loparic M, Wirz D, Daniels A U, Raiteri R, Vanlandingham M R, Guex G, Martin I, Aebi U and Stolz M 2010 Micro- and nanomechanical analysis of articular cartilage by indentation-type atomic force microscopy: validation with a gel–microfiber composite *Biophys. J.* 98 2731–40

Lyubchenko Y L, Gall A A, Shlyakhtenko L S, Harrington R E, Jacobs B L, Oden P I and Lindsay S M 1992 Atomic force microscopy imaging of double-stranded dna and rna *J. Biomolecular Struct. Dyn.* 10 589–606

Marikovsky Y, Resnitzky P and Reichman N 1978 Surface-charge characteristics of peripheral-blood lymphocytes in chronic lymphatic-leukemia and malignant-lymphoma *J. Natl Cancer Inst.* **60** 741–8

Martin-Palma R J, Manso M, Perez-Rigueiro J, Garcia-Ruiz J P and Martinez-Duart J M 2004 Surface biofunctionalization of materials by amine groups *J. Mater. Res.* 19 2415–20

Mitchison J and Swann M 1954 The mechanical properties of the cell surface. I: the cell elastimeter *J. Exp. Biol.* **31** 443–61

Moré J J 1978 *The Levenberg–Marquardt Algorithm: Implementation and Theory* ed G A Watson (Berlin: Springer) pp 105–16

Moreno-Herrero F, Colchero J and Baro A M 2003 DNA height in scanning force microscopy *Ultramicroscopy* 96 167–74

Moreno-Herrero F, Colchero J, Gomez-Herrero J and Baro A M 2004 Atomic force microscopy contact, tapping, and jumping modes for imaging biological samples in liquids *Phys. Rev.* E 69 031915

Müller D J and Dufrene Y F 2011 Atomic force microscopy: a nanoscopic window on the cell surface *Trends Cell Biol.* **21** 461–9

Ortega-Esteban A, Horcas I, Hernando-Perez M, Ares P, Perez-Berna A J, San Martin C, Carrascosa J L, De Pablo P J and Gomez-Herrero J 2012 Minimizing tip-sample forces in jumping mode atomic force microscopy in liquid *Ultramicroscopy* 114 56–61

Pablo D E, Colchero P J, J, Gomez-Herrero J and Baro A M 1998 Jumping mode scanning force microscopy *Appl. Phys. Lett.* 73 3300–2

Putman C A J, Vanderwerf K O, Degrooth B G, Vanhulst N F and Greve J 1994 Tapping mode atomic-force microscopy in liquid *Appl. Phys. Lett.* 64 2454–6

Putman C A J, Vanderwerf K O, Degrooth B G, Vanhulst N F and Greve J 1994 Viscoelasticity of living cells allows high-resolution imaging by tapping mode atomic-force microscopy *Biophys. J.* 67 1749–53

Radmacher M, Fritz M, Kacher C M, Cleveland J P and Hansma P K 1996 Measuring the viscoelastic properties of human platelets with the atomic force microscope *Biophys. J.* 70 556–67

Raman A, Trigueros S, Cartagena A, Stevenson A P Z, Susilo M, Nauman E and Contera S A 2011 Mapping nanomechanical properties of live cells using multi-harmonic atomic force microscopy *Nat. Nanotechnology* 6 809–14

Rico F, Roca-Cusachs P, Gavara N, Farre R, Rotger M and Navajas D 2005 Probing mechanical properties of living cells by atomic force microscopy with blunted pyramidal cantilever tips *Phys. Rev.* E 72 021914

Rodriguez A and Anderson J M 2010 Evaluation of clinical biomaterial surface effects on T lymphocyte activation *J. Biomed. Mater. Res.* A 92A 214–20

Russo A J, Howell J H, Han T, Bealmear P and Goldrosen M H 1979 Isolation of T-Cells, B-Cells and Macrophages by a 2-stage adherence procedure *J. Clin. Lab. Immunology* 2 67–72

Sader J E, Chon J W M and Mulvaney P 1999 Calibration of rectangular atomic force microscope cantilevers *Rev. Sci. Instrum.* 70 3967–9

Steward A, Toca-Herrera J L and Clarke J 2002 Versatile cloning system for construction of multimeric proteins for use in atomic force microscopy *Protein Sci.* 11 2179–83

Tang B and Ngan A H W 2011 Nanoindentation using an atomic force microscope *Phil. Mag.* 91 1329–38

Vie V, Giocondi M C, Lesniewska E, Finot E, Goudonnet J P and Le Grimellec C 2000 Tapping-mode atomic force microscopy on intact cells: optimal adjustment of tapping conditions by using the deflection signal *Ultramicroscopy* 82 279–88

Wang N, Butler J and Ingber D 1993 Mechanotransduction across the cell-surface and through the cytoskeleton *Science* 260 1124–7

Wu Y, Lu H, Cai J, He X, Hu Y, Zhao H and Wang X 2009 Membrane surface nanostructures and adhesion property of T lymphocytes exploited by AFM *Nanoscale Res. Lett.* 4 942–7

Yoffe E 1984 Modified Hertz theory for spherical indentation *Phil. Mag.* A 50 813–28

Zhou Z L, Ngan A H W, Tang B and Wang A X 2012 Reliable measurement of elastic modulus of cells by nanoindentation in an atomic force microscope *J. Mech. Behav. Biomed. Mater.* 8 134–42

Zhu C, Bao G and Wang N 2000 Cell mechanics: mechanical response, cell adhesion, and molecular deformation *Annu. Rev. Biomed. Eng.* 2 189–226